

Geophysical Research Letters[®]

RESEARCH LETTER

10.1029/2022GL100633

Key Points:

- Convective plumes penetrate downslope gravity currents and generate vertical interface fluctuations
- Vertical convective mixing erodes the stratified downslope flow and limits lateral transport
- The time of maximal lateral transport is delayed to the relaxation phase once penetrative convection weakens

Supporting Information:

Supporting Information may be found in the online version of this article.

Correspondence to:

T. Doda,
tomy.doda@eawag.ch

Citation:

Doda, T., Ulloa, H. N., Ramón, C. L., Wüest, A., & Bouffard, D. (2023). Penetrative convection modifies the dynamics of downslope gravity currents. *Geophysical Research Letters*, 50, e2022GL100633. <https://doi.org/10.1029/2022GL100633>

Received 3 AUG 2022
Accepted 20 DEC 2022






Author Contributions:

Conceptualization: T. Doda, H. N. Ulloa, C. L. Ramón, D. Bouffard
Data curation: T. Doda
Funding acquisition: D. Bouffard
Investigation: T. Doda, H. N. Ulloa, C. L. Ramón, D. Bouffard
Methodology: T. Doda, H. N. Ulloa, C. L. Ramón, D. Bouffard
Project Administration: D. Bouffard
Supervision: A. Wüest, D. Bouffard
Writing – original draft: T. Doda
Writing – review & editing: T. Doda, H. N. Ulloa, C. L. Ramón, A. Wüest, D. Bouffard

© 2023. The Authors.

This is an open access article under the terms of the [Creative Commons Attribution License](https://creativecommons.org/licenses/by/4.0/), which permits use, distribution and reproduction in any medium, provided the original work is properly cited.

Penetrative Convection Modifies the Dynamics of Downslope Gravity Currents

T. Doda^{1,2} , H. N. Ulloa^{2,3} , C. L. Ramón^{1,4} , A. Wüest^{1,2} , and D. Bouffard^{1,5} 

¹Eawag, Department of Surface Waters – Research and Management, Swiss Federal Institute of Aquatic Science and Technology, Kastanienbaum, Switzerland, ²Limnology Center, École Polytechnique Fédérale de Lausanne, Lausanne, Switzerland, ³Department of Earth and Environmental Science, University of Pennsylvania, Philadelphia, PA, USA, ⁴Department of Civil Engineering, University of Granada, Granada, Spain, ⁵Institute of Earth Surface Dynamics, University of Lausanne, Lausanne, Switzerland

Abstract Gravity currents contribute to the transport of heat and mass in atmospheric and aquatic environments. In aquatic systems subject to daily surface cooling, gravity currents propagate through turbulent convective surroundings. Yet, the effects of thermal convection on aquatic gravity currents remain to be quantified. This paper demonstrates how the interaction between penetrative convection and downslope gravity currents impacts the fluid dynamics and transport across littoral aquatic systems. We performed field experiments in a wind-sheltered lake experiencing differential cooling to resolve the dynamics of thermally driven gravity currents in convective environments. Our in situ observations reveal that convective plumes penetrate gravity currents, generating large vertical fluctuations that foster the erosion of the stratified layer. This enhanced vertical mixing destroys the stratified downslope flow and limits the basin-scale transport. Our results demonstrate that the interaction between penetrative convection and downslope gravity currents controls the littoral-pelagic connectivity in aquatic ecosystems.

Plain Language Summary Horizontal differences in fluid density generate flows called gravity currents. These currents transport heat and mass across environmental systems. The dynamics of gravity current and the resulting transport are well understood when the surroundings are quiescent, which is rarely the case in nature. In aquatic systems, turbulent processes such as convection energize the ambient water. Cooling-driven convection occurs when the surface of aquatic systems loses heat to the atmosphere, which generates sinking thermal plumes. In this paper, we used a lake experiencing differential cooling as an ideal field-scale laboratory to investigate the effects of convection on the dynamics of gravity currents. Our in situ observations reveal that convective plumes distort the upper interface of gravity currents and limit the flow intensity. These results demonstrate that convection constrains the horizontal transport induced by gravity currents in natural systems.

1. Introduction

Gravity currents are ubiquitous flows driven by horizontal density gradients across fluid environments (Benjamin, 1968; Huppert, 2006; Simpson, 1982). The dynamics of gravity currents were traditionally investigated via laboratory experiments assuming a quiescent ambient fluid (Britter & Linden, 1980; Ellison & Turner, 1959; Lofquist, 1960; Middleton, 1966). In nature, gravity currents often propagate through turbulent environments, energized, for example, by wind and thermal convection in the atmosphere (Dailey & Fovell, 1999; Ogawa et al., 2003; Serafin & Zardi, 2010), or by wind, tides, ambient currents, and waves in nearshore aquatic systems (Hetzel et al., 2015; Mahjabin et al., 2019; Ramón et al., 2022; Wright et al., 2001). Although the effects of ambient flows on the dynamics of gravity currents have been examined via laboratory and numerical experiments (Simpson & Britter, 1980; Bühler et al., 1991; C. Chen, 1995; A. J. Hogg et al., 2005), only a few studies have investigated the erosion and destruction of gravity currents by background turbulence (Harleman & Ippen, 1960; Linden & Simpson, 1986; Simpson, 1986).

Thermal convection is a pervasive and efficient turbulent mixing process in nature. It is driven by surface heating in the lower atmosphere (Hall et al., 1975; Stull, 1976) and by surface cooling in aquatic systems (Cushman-Roisin, 1982; Imberger, 1985), and it erodes stratified layers (Deardorff et al., 1969; Veronis, 1963) via plume penetration (Baines, 1975; Ching et al., 1993; Cotel & Kudo, 2008; Folkard, 2000; Noh et al., 1992). Although interactions between gravity currents and convection have been examined in the case of pyroclastic

flows (Huppert et al., 1986), double diffusive gravity currents (Maxworthy, 1983) and thermally driven winds (Dailey & Fovell, 1999; Ogawa et al., 2003; Serafin & Zardi, 2010), observations of such interactions are scarce in aquatic systems. An example of gravity currents flowing in the presence of penetrative convection in nearshore aquatic systems is the cross-shore overturning circulation driven by differential cooling between shallow and deep waters, aka thermal siphon (Horsch & Stefan, 1988; Monismith et al., 1990). By flowing downslope through the convective mixed layer, thermal siphons interact directly with convective plumes (Bednarz et al., 2008; Fer et al., 2002; Horsch & Stefan, 1988). We recently hypothesized from field observations (Doda et al., 2022) and numerical simulations (Ulloa et al., 2022) that vertical mixing by convective plumes might destroy thermal siphons and we expressed the need for further investigations of the effects of convective surroundings on gravity current dynamics. Here, we fill this gap by conducting fine spatiotemporal measurements of thermal siphons in a wind-sheltered lake. By analyzing global and local parameters under different thermal forcing scenarios, we show that the intensity of penetrative convection controls the vertical mixing and the hydrodynamic stability of the thermally stratified downslope flow. Thus, in contrast to classical gravity currents in quiescent environments, gravity currents propagating through convective turbulence experience an abrasive degeneration that diminishes the horizontal exchange across nearshore waters.

2. Methods

2.1. Field Experiments and Measurements

In situ observations of thermal siphons were conducted in Rotsee (Switzerland), an elongated wind-sheltered lake (Figure S1 in Supporting Information S1). The northeastern end of the lake is characterized by a shallow plateau that fosters daily thermal siphons from summer to winter (Doda et al., 2022). Such flows develop several hours after the cooling phase starts, once the fluid inertia balances lateral density gradients induced by differential cooling (Doda et al., 2022; Ulloa et al., 2022). Here, we investigate the dynamics of gravity currents on the plane (x, z) , where x is the cross-shore direction along the thalweg, and z is the vertical direction (Figure 1a).

We measured thermal siphons propagating from the northeastern end toward the lake interior from July to December 2019. Measurements are briefly described below, and we refer to Doda et al. (2022) for further details about the setup and accuracy of the instruments. Meteorological forcing was resolved by a weather station installed near the plateau region. Four moorings M1–M4 were deployed along the lake thalweg at depths of 2.2, 4, 13, and 16 m, respectively (Figure 1a). M2 and M4 provided seasonal-scale water temperature and velocity measurements in the sloping zone off the plateau region (M2, slope of 1.5°) and near the deepest point (M4). M2 was composed of a vertical thermistor array and an up-looking acoustic Doppler current profiler (ADCP, Nortek Aquadopp profiler 1 MHz). The ADCP profiled the water column from 0.25 to 3 m above the bottom, with a vertical bin resolution of 0.05 m. Every 15 min, it collected 4.3 min-long bursts of 512 velocity samples at 2 Hz. M4 monitored the lake thermal structure with a vertical thermistor array. The other thermistor arrays M1 and M3 were deployed during short-term campaigns in autumn 2019. We collected conductivity-temperature-depth (CTD, Sea&Sun Technology CTD60M) profiles at 13 points along the same cross-shore transect, from P01 (1.3 m deep, 190 m from the shore) to P13 (M4, 800 m offshore from P01). We also profiled the water column at M2 every 15 min on November 6–7, 2019.

2.2. Data Analysis

Surface heat and buoyancy fluxes were estimated from the meteorological data and surface temperature at M4 (Doda et al., 2022). The net surface buoyancy flux was computed as $B_{0,\text{net}} = B_{\text{SW},0} + B_0$, where $B_{\text{SW},0}$ and B_0 are the shortwave and non-penetrative fluxes, respectively.

We computed the vertical density structure over time at each mooring by applying the equation of state from C.-T. A. Chen and Millero (1986) to convert temperature into density by assuming constant salinity of $S = 0.2 \text{ g kg}^{-1}$ (Doda et al., 2022). The average surface densities ρ_{M1} and ρ_{M3} were estimated over the upper 1.5 m at M1 and over the upper 2.0 m at M3, respectively. We calculated the cross-shore density gradient caused by differential cooling/heating as $\partial_x \rho = (\rho_{\text{M3}} - \rho_{\text{M1}})/\Delta x$, where $\Delta x = x_{\text{M3}} - x_{\text{M1}} = 400 \text{ m}$ is the cross-shore distance between the two moorings.

We applied the algorithm introduced by Doda et al. (2022) to detect thermal siphons and compute their cross-shore velocity u . The thickness of gravity currents over time $h_d(t)$ at M2 was estimated as the length between the sediment-water interface and the stagnation point $u(h_d, t) = 0$. Cross-shore transects of temperature profiles

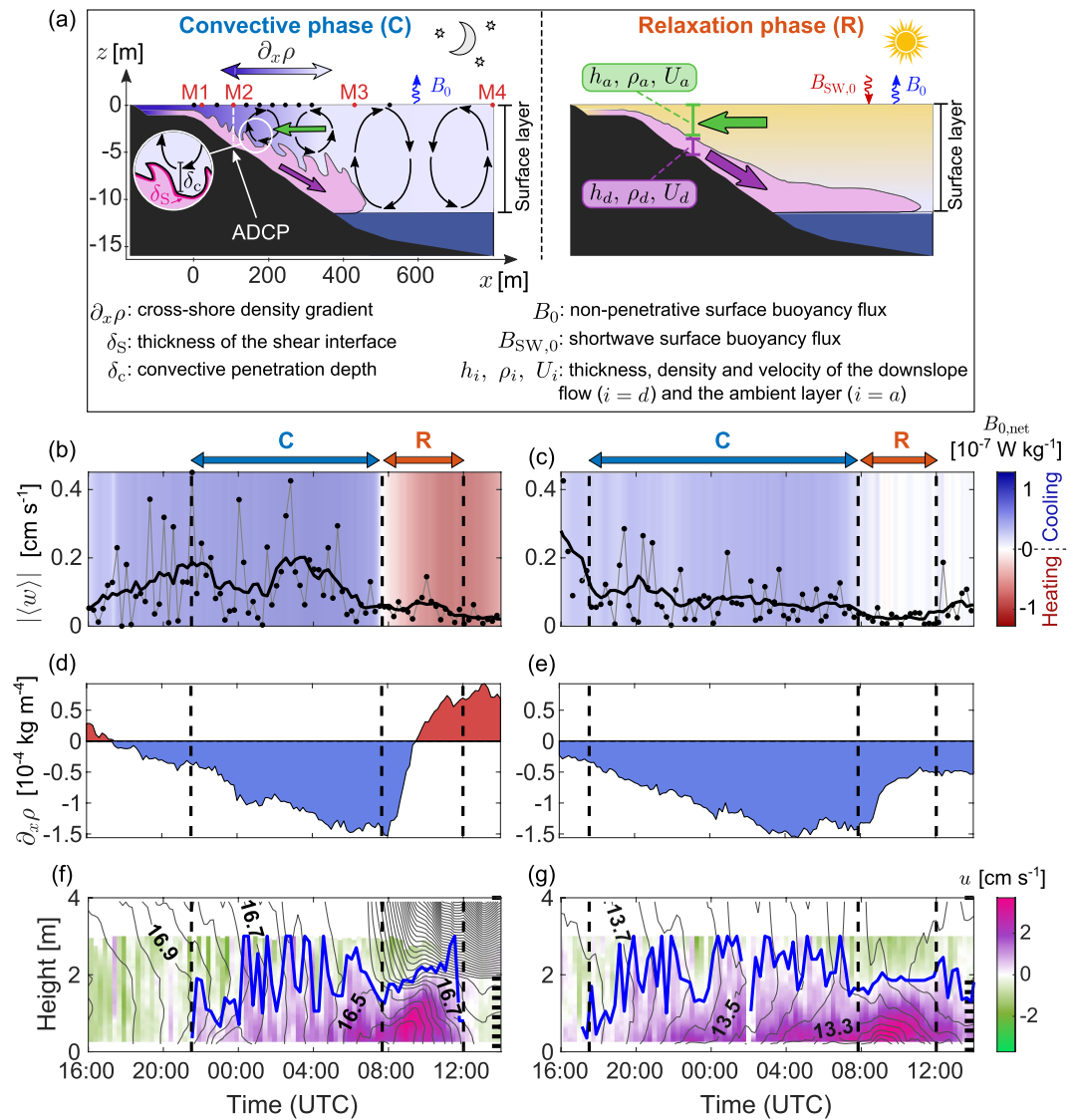


Figure 1. Diurnal phases for two different thermal siphon events in 2019. (a) Schematic of the night-time convective (C) phase and daytime relaxation (R) phase along the lake thalweg. Black arrows represent convective plumes. Dots at the lake surface depict the location of conductivity-temperature-depth (CTD) profiles on 6–7 November with moorings in red. (b–g) Time series of (b and c) surface net buoyancy flux (shading) and depth-averaged vertical velocity at M2 (black dots are burst-averaged values and the black line is the 2-hr moving average), (d and e) lateral surface density gradient caused by differential cooling/heating between M1 and M3, and (f and g) burst-averaged cross-shore velocity at M2 as a function of height above the sediment. Blue lines in (f) and (g) show the upper interface of the gravity current h_d . Gray lines are 0.05°C-spaced isotherms, linearly interpolated between thermistors (black ticks on the right vertical axis). Offshore (onshore) velocities are defined positive (negative). (b, d, f) correspond to 10–11 October (cooling-heating case) and (c, e, g) to 6–7 November (continuous-cooling case).

allowed tracking the bottom stratification induced by gravity currents along x . From each temperature profile $T(z)$, we estimated the current's thickness $h_{d,T}$ as the height above the bottom, where $dT/dz < 0.03^\circ\text{C m}^{-1}$. The latter gradient threshold was chosen such that $h_{d,T} \approx h_d$ when h_d was steady at M2.

2.3. Scaling and Dimensionless Numbers

We consider a two-layer exchange flow, with a downslope stratified current of thickness h_d , density ρ_d , and cross-shore velocity $U_d > 0$ and an upper ambient layer of thickness h_a , density $\rho_a < \rho_d$ and cross-shore velocity $U_a < 0$ (Figure 1a). The density and velocity of each layer are depth-averaged over h_d and h_a at M2. The depth of the interface between the two layers is $z_d = -h_a = h_d - h_{max}$, where $h_{max} \approx 4$ m is the maximum depth at M2.

The downslope flow regime is characterized by the densimetric Froude number Fr_D , expressing the ratio of kinetic to potential energy as (Ellison & Turner, 1959)

$$Fr_D^2 = \frac{1}{Ri_B} = \frac{(U_d - U_a)^2}{g' h_d \cos \theta}, \quad (1)$$

where Ri_B is the bulk Richardson number, $g' = g(\rho_d - \rho_a)/\rho_0$ is the reduced gravity of the density current, $\rho_0 = 1,000 \text{ kg m}^{-3}$ is the reference density, and $\theta = 1.5^\circ$ is the slope angle. We neglect the slope effects in the following analysis since $\cos \theta \approx 1$. The upper interface dynamics of turbulent gravity currents depend on Fr_D , with larger interface distortions for higher Fr_D (Salinas et al., 2020). We use here a critical Froude number of $Fr_D^{(\text{crit})} = 1$ to normalize Fr_D (Ellison & Turner, 1959; Salinas et al., 2020). Although other definitions of $Fr_D^{(\text{crit})}$ (Huang et al., 2009) or other Froude numbers (Armi, 1986; Thorpe & Ozen, 2007; Waltham, 2004) could be used, they would not affect relative changes in Fr_D over time. The interface stability to shear disturbances can be investigated with the gradient Richardson number

$$Ri_g = -\frac{g}{\rho_0} \frac{\partial \rho / \partial z}{(\partial u / \partial z)^2}, \quad (2)$$

where shear instabilities grow when $Ri_g < Ri_g^{(\text{crit})} = 0.25$ (Miles, 1961). Here, we use both Fr_D and the gradient Richardson number at z_d $Ri_{g,\text{int}} = Ri_g(z = z_d)$ to characterize shear effects on the interface dynamics at M2.

Based on previous studies on plume impingement at stratified interfaces (Baines, 1975; Cotel & Kudo, 2008; Noh et al., 1992), we quantify the relative intensity of penetrative convection with respect to the stratified downslope flow with the convective Richardson number

$$Ri_c = \frac{g' h_a}{W_a^2}, \quad (3)$$

with $W_a = 1/h_a \int_{-h_a}^0 w(z) dz$ the depth-averaged vertical velocity in the ambient layer. A change of convective regime has been reported at a critical value of $Ri_c^{(\text{crit})} \approx 10$, below which plumes penetrate across the stratified interface (Cotel & Kudo, 2008; Noh et al., 1992). We further define the penetration depth of convective plumes as

$$\delta_c = \frac{|W_a|}{N_d}, \quad (4)$$

where $N_d = \sqrt{\langle -g/\rho_0 (\partial \rho / \partial z) \rangle_{z < z_d}}$ is the depth-averaged buoyancy frequency in the gravity current. To examine whether convection dominates over shear-driven disturbance across the current interface, we compare δ_c with the thickness of shear (δ_s) and density (δ_ρ) interfaces defined from the maximum velocity and density gradients as (Zhu & Lawrence, 2001):

$$\delta_s = \frac{(U_d - U_a)}{(\partial u / \partial z)_{\text{max}}}, \quad (5)$$

and

$$\delta_\rho = \frac{(\rho_d - \rho_a)}{(\partial \rho / \partial z)_{\text{max}}}. \quad (6)$$

If $\delta_c > \delta_s, \delta_\rho$, convective plumes penetrate beyond the current interface defined from shear and density and erode the stratified layer.

3. Results

3.1. Diurnal Cycle

We investigate the effect of penetrative convection on gravity currents by examining two distinctive thermal siphon events (Figure 1). The first event (October 10–11, 2019) is a canonical scenario expected in the early autumn when the diurnal cycle has well-defined cooling and heating phases that constrain the development of thermal siphons. In contrast, the second event (November 6–7, 2019) represents a persistently cold late-autumn day, with a continuously flowing thermal siphon. We hereafter refer to these scenarios as the cooling-heating and continuous-cooling cases, respectively. Despite the differences in the thermal forcing, both scenarios show

two remarkable dynamic regimes: (a) a nighttime convective (C) phase, during which convective plumes interact with the gravity current; (b) a daytime relaxation (R) phase, during which penetrative convection weakens and the gravity current intensifies.

We found that during the C-phase, surface cooling (net surface buoyancy flux $B_{0,\text{net}} \approx 10^{-7} \text{ W kg}^{-1}$) caused convective mixing with depth-averaged vertical velocities of $\langle w \rangle \approx 10^{-1} \text{ cm s}^{-1}$ (black line in Figures 1b and 1c). At the same time, a negative cross-shore density gradient developed by differential cooling, which increased in time until reaching a quasi-steady magnitude of about $\partial_x \rho \approx -1.5 \times 10^{-4} \text{ kg m}^{-4}$ (Figures 1d and 1e). The thermally driven gravity current was weakly stratified (squared buoyancy frequency $N_d^2 < 10^{-4} \text{ s}^{-2}$) and unsteady, with up to $\sim 2 \text{ m}$ vertical fluctuations at its upper interface (blue line in Figures 1f and 1g). The transition from the C-phase to the R-phase occurred at sunrise when the net cooling heat flux diminished and the intensity of convection weakened. This caused a sudden drop of $|\partial_x \rho|$ and a baroclinic adjustment with an intensification of the downslope gravity current (Figures 1f and 1g). In early autumn, strong radiative heating stratified the surface layer (Figure 1f), which was not observed in late autumn (Figure 1g). Despite having different forcing conditions, the current dynamics during the C- and R-phases were similar between the two scenarios. We remark that vertical fluctuations at the interface swiftly vanished and horizontal circulation intensified (Figures 1f and 1g) once vertical velocity dropped during the R-phase (Figures 1b and 1c), suggesting that thermal plumes modified the current dynamics.

3.2. Interface Dynamics of the Gravity Current

We further examined the dynamical regime shift from the C-phase to the R-phase using high-frequency velocity bursts. We compared two 4 hr-long sub-periods from each phase of the continuous-cooling scenario (Figure 2). Although the average thickness of the gravity current was $\overline{h_d} \approx 2 \text{ m}$ for both phases, the variability of h_d was more than four times larger during the C-phase with a standard deviation of 0.70 m, compared to 0.15 m during the R-phase. Fluctuations of $|h'_d| = |h_d - \overline{h_d}| \approx 1 \text{ m}$ indicated vigorous vertical mixing during the C-phase (Figure 2c) and patches of positive u observed above the main interface suggested detrainment of the downslope flow into the upper layer (Figure 2a). During this turbulent phase, vigorous convective downdrafts and updrafts ($|w| \approx 0.5 \text{ cm s}^{-1}$) penetrated across the current interface (Figure 2b). The penetration depth was $\delta_c \approx 0.1\text{--}1 \text{ m} > \delta_s, \delta_\rho$ (Equations 4–6, Figure 2d) during the C-phase. In contrast, the combined effect of low vertical velocity fluctuations and strong near-bottom stratification prevented the erosion of the downslope gravity current during the R-phase, with $\delta_c \approx 10^{-2} \text{ m} < \delta_s, \delta_\rho$. These observations indicate that the convective regime shift between C- and R-phases modified the intensity of (a) the vertical mixing between the downslope current and the ambient fluid and (b) the cross-shore flow.

To identify distinctive dynamic properties of the C- and R-phases for the cooling-heating and continuous-cooling scenarios, we computed the probability density function of six parameters associated with the strength of the bottom layer stratification, and the destabilizing effects of penetrative convection and shear (Figure 3). For both scenarios, the gravity current changed its dynamics between the C- and R-phases, with one-order of magnitude smaller vertical fluctuations $|h'_d|/\overline{h_d}$ and a stronger and less variable stratification $N_d^2 \overline{h_d}/g'_\text{max}$ during the R-phase (Figures 3a and 3b). The magnitudes of $|h'_d|/\overline{h_d}$ and N_d^2 in the C- and R-phases were the same between the two forcing scenarios. The two scenarios also showed a similar change in the convective regime (Figures 3c and 3d). From the C-phase to the R-phase, the mean convective Richardson number Ri_c increased by two orders of magnitude and the mean ratio δ_c/δ_s dropped by one order of magnitude from $\sim 10^{0.5}$ to $\sim 10^{-0.5}$. Such striking changes in Ri_c and δ_c/δ_s confirm that the shift in current dynamics resulted from a weakening of penetrative convection. On average, the flow was close to critical conditions ($\text{Fr}_D/\text{Fr}_D^{(\text{crit})} \approx 1$; Figure 3e) and marginally stable ($\text{Ri}_{g,\text{int}}/\text{Ri}_g^{(\text{crit})} \approx 1$; Figure 3f). Although the surface stratification during the R-phase of the cooling-heating case led to a decrease in Fr_D and an increase in $\text{Ri}_{g,\text{int}}$ compared to the C-phase, such a shift was not observed for the continuous-cooling case. The absence of a consistent shift of Fr_D and $\text{Ri}_{g,\text{int}}$ between the C- and R-phases implies that shear was not responsible for the substantial change in the gravity current dynamics.

3.3. Structure and Propagation of the Gravity Current

The vertical density structure and the propagation of the stratified downslope flow during the continuous-cooling scenario were analyzed from density inferred from temperature profiles (Figure 4). Active convection fostering vertical mixing during the C-phase led to a weakly stratified downslope flow (vertical density gradient $\partial \rho / \partial z \approx -0.01 \text{ kg m}^{-4}$, Figure 4a). The near-bottom stratification was spatially variable and dropped to

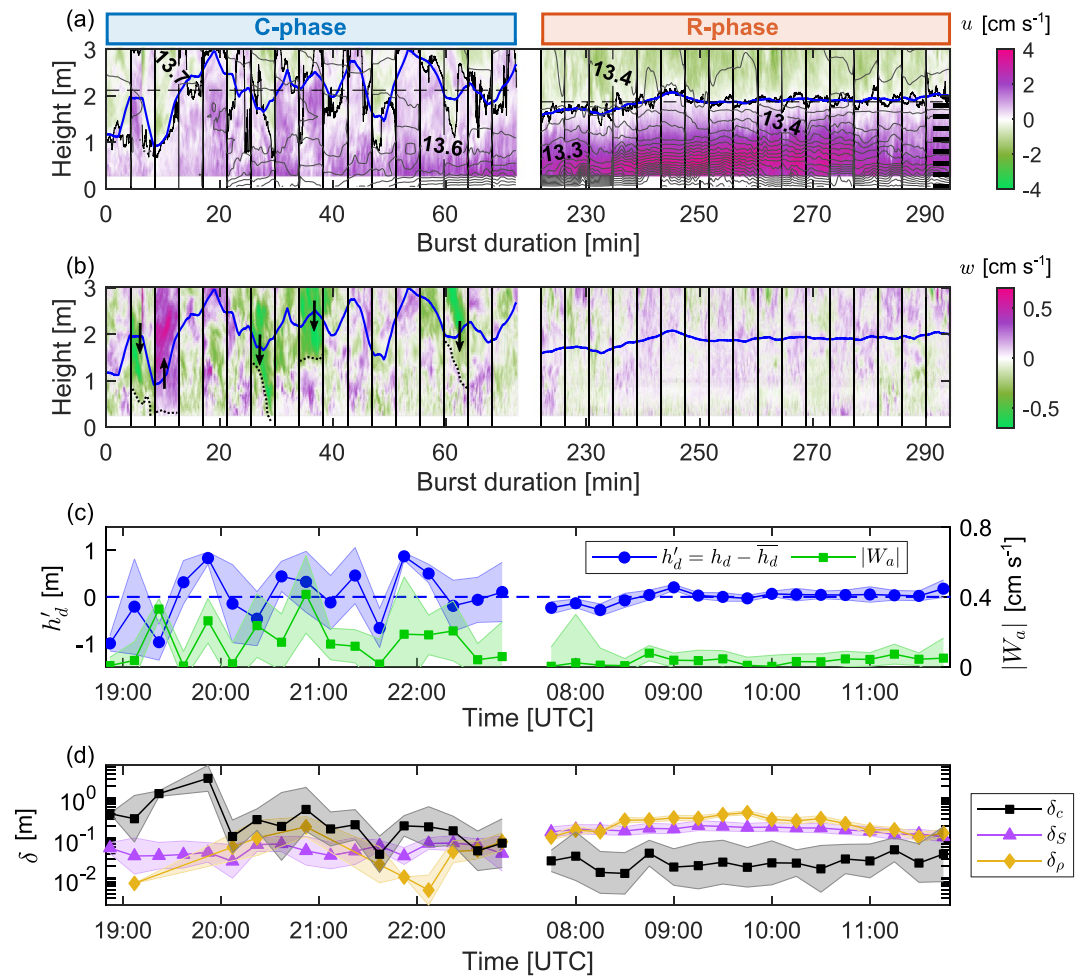


Figure 2. Subsets of the convective and relaxation phases captured in the sloping region (M2) on 6–7 November. (a) High frequency cross-shore velocity over the three first meters above the sediment as a function of time. The bursts are combined together and delimited by vertical black lines. The time is expressed as the burst duration since the first sample. Solid black and blue lines depict the high-frequency and smoothed upper interface of the gravity current, respectively. The dashed horizontal line indicates the average thickness \bar{h}_d during each subset. Gray lines are 0.02°C -spaced isotherms, linearly interpolated between the thermistors (black ticks on the right vertical axis). (b) Same as (a) for the vertical velocity. Arrows highlight strong convective downdrafts and updrafts that penetrate across the interface. Their penetration depth is qualitatively shown with dotted lines. The blue line is identical to (a). (c) Burst-averaged time series of interface fluctuations h'_d and depth-averaged vertical velocity in the ambient layer $|W_d|$. (d) Burst-averaged time series of penetrative length scale δ_c , shear interface thickness δ_s , and density interface thickness δ_ρ . Shaded areas in (c) and (d) show the standard deviation for each burst-average.

$\partial\rho/\partial z \approx -0.001 \text{ kg m}^{-4}$ for $x > 200 \text{ m}$. On average, only the lower 1.5 m at the sloping region (M2) were stratified, which represented $h_{d,T}/h_d \approx 60\%$ of the gravity current thickness (Figure 4b). The velocity maximum was located close to the bottom boundary, at $h_{U_d,\text{max}} < 0.15 h_d$, and not captured by the ADCP. During the R-phase, $h_{d,T}$ increased at all locations, and the intrusion of cold water was observed at the base of the mixed layer for $x > 400 \text{ m}$ (Figure 4c). The gravity current became vertically stratified from its base to its upper interface ($h_d \approx h_{d,T}$), and the height of maximal velocity increased to $h_{U_d,\text{max}} \approx 0.25 h_d$ (Figure 4d). The strengthening of flow velocity and stratification once convection weakens suggest that vertical mixing during the C-phase eroded the downslope density current and reduced the lateral transport.

4. Discussion

By comparing the dynamics of thermal siphons in the presence and absence of convective plumes, this study pinpoints the effects of penetrative convection on the structure and propagation of a thermally driven gravity current.

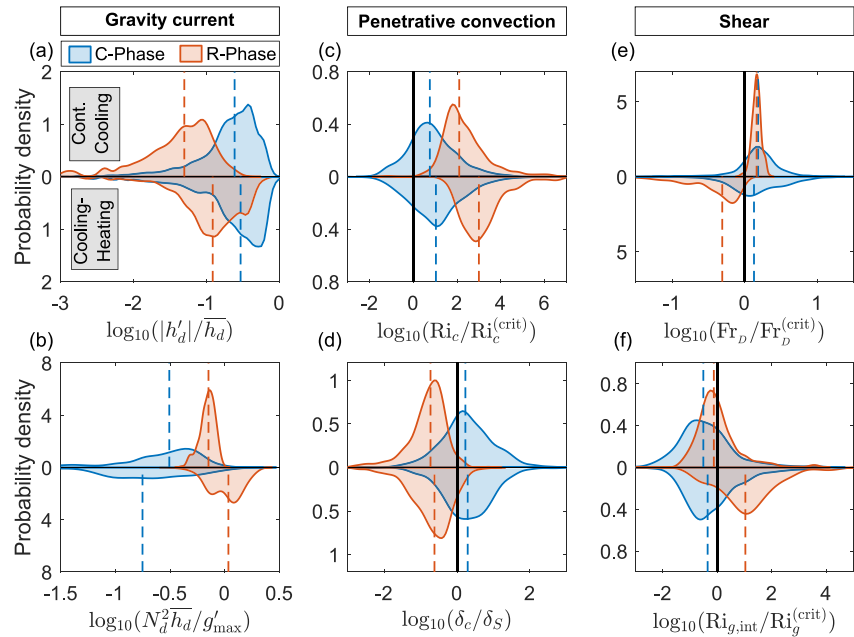


Figure 3. Probability density plots comparing the convective (blue) and relaxation (orange) phases, for the cooling-heating and continuous-cooling scenarios (lower and upper part of each panel, respectively). (a) Vertical fluctuations of the interface h'_d normalized by the mean current thickness \bar{h}_d . Large fluctuations, with h_d thicker than the acoustic Doppler current profiler (ADCP) profiling range (3 m), are not included. (b) Dimensionless squared buoyancy frequency of the gravity current, where $g'_{\max} = g |\partial_x \rho|_{\max} \Delta x / \rho_0 = 5.9 \times 10^{-4} \text{ m s}^{-2}$ is the reduced gravity from the maximum absolute lateral gradient $|\partial_x \rho|_{\max} = 1.5 \times 10^{-4} \text{ kg m}^{-4}$ (Figure 1). (c) Convective Richardson number normalized by $\text{Ri}_c^{(\text{crit})} = 10$. (d) Ratio of penetrative length scale to the shear interface thickness. (e) Densimetric Froude number normalized by $\text{Fr}_D^{(\text{crit})} = 1$. (f) Interfacial gradient Richardson number normalized by $\text{Ri}_g^{(\text{crit})} = 0.25$. In (c, e, f) only positive values are included, corresponding to a stable stratification. The vertical black solid line in (c)–(f) indicates a ratio of one. Vertical dashed lines show the median values over each phase.

When convective plumes penetrated across the interface of the downslope flow during the C-phase, we found that (a) the interface of the gravity current experienced large vertical fluctuations and (b) the dynamic bottom layer of positive cross-shore velocity was only partially stratified. This partial stratification differed, for instance, from the density structure resulting from lock-exchange gravity currents, for which the maximum shear and maximum density gradient coincide and $h_{U_{d,\max}}/h_d \approx 0.2$ (Ellison & Turner, 1959; Thorpe & Ozen, 2007; Wells & Dorrell, 2021). Conversely, in the absence of penetrative convection and vigorous vertical mixing during the R-phase, the downslope flow showed a more stable interface, and it recovered the canonical structure of gravity currents.

4.1. Role of Convection in the Small-Scale Interface Dynamics

At low Ri_c , the impingement of plumes and thermals deflects stratified interfaces (Baines, 1975; Ching et al., 1993; Cotel & Kudo, 2008; Noh et al., 1992), as observed in convective boundary layers (Deardorff et al., 1969; Stull, 1976). During the C-phase, Ri_c varied over six orders of magnitude due to the temporal fluctuations of W_a and was statistically larger than $\text{Ri}_c^{(\text{crit})} = 10$ (Figure 3c). Yet, if we focus on intense convective episodes by including negative Ri_c (Figure S2 in Supporting Information S1) and discarding weak convective periods (depth-averaged vertical velocity in the ambient layer $W_a < 1 \times 10^{-3} \text{ m s}^{-1}$), we found that $\text{Ri}_c \lesssim \text{Ri}_c^{(\text{crit})}$ (interquartile intervals of $-8 < \text{Ri}_c < 25$ and $-5 < \text{Ri}_c < 25$ for the cooling-heating and continuous-cooling scenarios, respectively). Sullivan et al. (1998) showed that convective updrafts (downdrafts) push the boundary layer interface locally upward (downward). Such interface fluctuations are linked to the penetration depth δ_c and the convective Richardson number as $\sigma_{h_a}/\bar{h}_a \sim \delta_c/\bar{h}_a \sim \text{Ri}_c^{-\gamma}$, where σ_{h_a} and \bar{h}_a are the standard deviation (similar to $|h'_d|$) and mean of the convective layer thickness, with $\gamma \approx 1$ (Ching et al., 1993; Cotel & Kudo, 2008; Noh et al., 1992). For $\text{Ri}_c \approx 10$ and $\bar{h}_a \approx 1 \text{ m}$, the standard deviation σ_{h_a} scales with the penetration depth, that is, $\sigma_{h_a} \approx \delta_c \approx 0.1 \text{ m}$, which is the same order of magnitude as the fluctuations $|h'_d|$ (Figure 2). Yet, this $\text{Ri}_c \cdot \sigma_{h_a}$

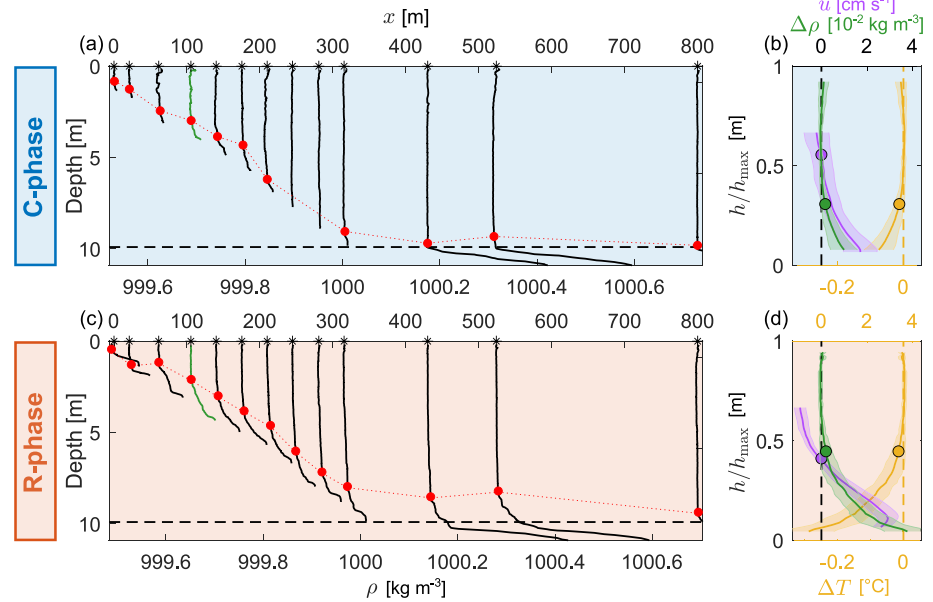


Figure 4. Cross-shore propagation of the gravity current during the convective and relaxation phases on 6–7 November. (a and c) Cross-shore transect of density profiles inferred from temperature profiles P01–P13, as a function of distance x from P01, for (a) the convective phase (period 03:33–04:51 UTC), and (c) the relaxation phase (period 09:43–10:39 UTC). Each density profile P_i is shifted proportionally to the distance x_{P_i} from P01 (black stars on the x axis), as $\tilde{\rho}_{P_i} = \rho_{P_i} + x_{P_i} \times 0.0015 \text{ kg m}^{-4}$, where ρ_{P_i} and $\tilde{\rho}_{P_i}$ are the measured and shifted densities, respectively. The density profile at M2 is shown in green. The horizontal dashed line depicts the base of the mixed layer at M4. Red dots indicate the upper interface of the gravity current $h_{d,T}$. (b and d) Average profiles of cross-shore velocity (purple), density anomaly (green), and temperature anomaly (yellow) as a function of dimensionless height at M2, for (b) the convective phase (17:30–07:50 UTC) and (d) the relaxation phase (07:50–12:00 UTC). The density anomaly is computed from the temperature anomaly $\Delta T(z) = T(z) - T_0$, where T_0 is the median temperature above $h_{d,T}$. Shaded area on each profile represents the standard deviation. Dots depict the upper interface of the gravity current, from the stagnation point (h_d , purple dot) and temperature gradient ($h_{d,T}$, green and yellow dots).

relationship was derived for a horizontally “stationary” stratified interface interacting with vertical plumes, which differs from our case where both the stratified and ambient layers are actively streaming in the horizontal direction. The horizontal flow modifies the plume trajectory and penetration, which could explain the weak relationship between the current dynamics at M2 and the local Ri_c ($\gamma \approx 0.1$, Figure S3 in Supporting Information S1). The observed small-scale dynamics may also integrate fluctuations generated by convectively forced internal waves (Ansong & Sutherland, 2010; Fritts & Alexander, 2003), shear instabilities (Pawlak & Armi, 2000; Zhu & Lawrence, 2001), and pulses and roll waves (Alavian, 1986; Dressler, 1949; Fer et al., 2001; Needham & Merkin, 1984). However, the absence of a consistent shift of Ri_g and Fr_D between the C- and R-phases (Figures 3e and 3f) suggests that shear instabilities and roll waves play a secondary role in the current dynamics. The dominant period of the fluctuations $T_{h'_d} \approx 1 \text{ h}$ (Figure 1) does not match the characteristic periodicity of pulses (Table S1 in Supporting Information S1), but agrees with the duration of a convective overturn $\tau_c = 2 \cdot h_d / |W_d| \approx 1 \text{ hr}$, where $h_d \approx 2 \text{ m}$ and $|W_d| \approx 1 \times 10^{-3} \text{ m s}^{-1}$. Therefore, penetrative convection arises to be the primary cause of the fluctuating dynamics observed during the C-phase.

4.2. Role of Convection in the Basin-Scale Lateral Transport

The erosion of the stratified downslope flow by convective plumes (Figure 4) was comparable to the effects of turbulence on fronts propagation (Linden & Simpson, 1986; Simpson, 1986) and exchange flows (A. M. Hogg et al., 2001). Linden and Simpson (1986) found that the front velocity of lock-exchange gravity currents experiencing turbulent mixing was less than the velocity scale U_s based on horizontal density gradients in a quiescent environment. In our case, $U_s = 0.5 \sqrt{-g \partial_x \rho \Delta x h_{lit} / \rho_0} \approx 1.7 \text{ cm s}^{-1}$, where $\Delta x = 400 \text{ m}$ is the cross-shore distance along which $\partial_x \rho \approx -1 \times 10^{-4} \text{ kg m}^{-4}$ was computed (Figure 1) and $h_{lit} \approx 3 \text{ m}$ is the mean depth of the littoral region experiencing $\partial_x \rho$. The averaged downslope velocity during the R-phase $U_d \approx 1.5 \pm 0.4 \text{ cm s}^{-1} \approx 0.9 U_s$ matched the

scale U_s . In the presence of convection during the C-phase, however, it was only $U_d \approx 0.8 \pm 0.3 \text{ cm s}^{-1} \approx 0.5 U_s$ —consistent with Linden and Simpson (1986). The authors found that the flow became vertically mixed after a distance L_x and ran out of energy to propagate further. We posit that the propagation distance is controlled by penetrative convection during the C-phase and scales as $L_x \sim U_s h_d / w_e$, where $w_e = A W_d / \text{Ri}_c = A B_0 h_d / (g' h_d)$ is the convective entrainment velocity, with A an empirical coefficient (Deardorff et al., 1980). This distance represents how far the gravity current propagates before being entirely eroded by penetrative plumes. Considering $g' \sim g \partial_x \rho \Delta x / \rho_0 \approx 4 \times 10^{-4} \text{ m s}^{-2}$, $h_d \approx h_a \approx 2 \text{ m}$, $B_0 \approx 1 \times 10^{-7} \text{ W kg}^{-1}$, and $A \approx 0.2$ (Sullivan et al., 1998), we obtain $L_x \approx 0.5 g'^{3/2} h_{\text{lit}}^{1/2} h_d^2 / (A B_0 h_a) \approx 700 \text{ m}$. The order of magnitude $L_x \approx 10^2\text{--}10^3 \text{ m}$ is consistent with our observations of complete mixing at around $x \approx 250 \text{ m}$ from P01 (Figure 4a), equivalent to $L_x \approx 200 + x = 450 \text{ m}$ from the shore. The degeneration of the downslope stratified layer before reaching the lake interior confirms the numerical results by Ulloa et al. (2022).

Convective mixing may also modify the growth of the gravity current by entrainment. The net shear entrainment of ambient water into a gravity current is expressed by $E_{\text{net}} = \partial_x(U_d h_d) / (U_d - U_a)$, which has been parametrized as a function of the bulk Richardson number Ri_B in quiescent environments (Cenedese & Adduce, 2010; Ellison & Turner, 1959). Fer et al. (2002) suggested that convective plumes increase E_{net} in thermal siphons, but their estimate of E_{net} did not include the effects of the large Reynolds number $\text{Re} \approx 10^5$. Although we observed a thinner stratified layer in the presence of penetrative convection (Figure 4), we cannot infer the effects of convective plumes on the downstream evolution of the discharge ($U_d h_d$) from a single-point measurement. We encourage future studies to quantify the contribution of convective plumes to the net entrainment by comparing estimates of E_{net} between the C- and R-phases. Such estimates could be obtained from simultaneous discharge measurements at several locations along a cross-shore transect. We stress that the effects of the return flow must be included since $h_d/h_a \approx 1$ as in counterflows (Christodoulou, 1986; Moore & Long, 1971).

During the C-phase, vertical fluxes between the downslope flow and the ambient layer were enhanced by convective mixing, which diluted transported tracers and diminished the cross-shore exchange. A similar reduction in the lateral transport of tracers due to turbulent diffusion has been reported for exchange flows (Helfrich, 1995; A. M. Hogg et al., 2001; Winters & Seim, 2000). The maximal transport was observed during the R-phase or heating phase in Rotsee (Doda et al., 2022), in agreement with numerical simulations of thermal siphons (Chubarenko et al., 2013; Safaie et al., 2022). This relaxation is comparable to the frontogenesis observed by Linden and Simpson (1986) once turbulence was turned off. The intensification of gravity currents with weaker turbulent mixing has also been observed in the atmosphere (Parker et al., 2005; Sha et al., 1991; Simpson et al., 1977) and estuaries (Hetzl et al., 2015). Although thermal siphons are traditionally perceived as a nocturnal transport process (Brothers et al., 2017), our results show that penetrative convection delays the time of maximal transport to daylight conditions. Accounting for this delay is essential to quantify the ecological implications of thermal siphons in aquatic systems.

5. Conclusion

The dynamics of downslope flows induced by differential cooling result from the intimate interaction between penetrative convection and gravity currents. Our high-resolution observations demonstrate that convective plumes modify the small-scale dynamics and the basin-scale propagation of gravity currents by vertical mixing. Due to the rich fluid dynamics driven by differential cooling, in which shear and convective flows coexist, further investigations of thermal siphons would expand our understanding of gravity currents in convective surroundings. Our study highlights the need for a holistic understanding of geophysical flows that integrates the various interactions between physical processes.

Conflict of Interest

The authors declare no conflicts of interest relevant to this study.

Data Availability Statement

Our in situ data can be used by experimentalists and modellers for further investigations. It is available for download, along with scripts used for data processing, analyses and plots, at: <https://doi.org/10.25678/0007PR>.

Acknowledgments

We sincerely thank our technician, Michael Plüss, for supervising the field campaigns. We acknowledge Kathrin Baumann, Bieito Fernández-Castro, Sébastien Lavanchy and Love Råman Vinnå for their help in the field. We are grateful to the Canton of Luzern, the municipalities of Luzern and Ebikon, the Rowing Centre Lucerne-Rotsee, the Quartierverein Maihof and Pro Natura associations, and the Rotsee-Badi for supporting us in our measurements. We thank Kraig Winters, Oscar Sepúlveda Steiner, Marco Toffolon, Martin Schmid, and Gregory Lawrence for discussions and comments on the manuscript. Finally, we acknowledge the two anonymous reviewers for their constructive comments that improved this manuscript. This study was financed by the Swiss National Science Foundation (“Buoyancy driven nearshore transport in lakes” project; HYPOlimnetic THERmal SiphonS, HYPOTHESIS, Grant 175919).

References

- Alavian, V. (1986). Behavior of density currents on an incline. *Journal of Hydraulic Engineering*, 112(1), 27–42. [https://doi.org/10.1061/\(ASCE\)0733-9429\(1986\)112:1\(27\)](https://doi.org/10.1061/(ASCE)0733-9429(1986)112:1(27))
- Ansong, J. K., & Sutherland, B. R. (2010). Internal gravity waves generated by convective plumes. *Journal of Fluid Mechanics*, 648, 405–434. <https://doi.org/10.1017/S0022112009993193>
- Armi, L. (1986). The hydraulics of two flowing layers with different densities. *Journal of Fluid Mechanics*, 163, 27–58. <https://doi.org/10.1017/S0022112086002197>
- Baines, W. D. (1975). Entrainment by a plume or jet at a density interface. *Journal of Fluid Mechanics*, 68(2), 309–320. <https://doi.org/10.1017/S0022112075000821>
- Bednarz, T. P., Lei, C., & Patterson, J. C. (2008). An experimental study of unsteady natural convection in a reservoir model cooled from the water surface. *Experimental Thermal and Fluid Science*, 32(3), 844–856. <https://doi.org/10.1016/j.exthermflusci.2007.10.007>
- Benjamin, T. B. (1968). Gravity currents and related phenomena. *Journal of Fluid Mechanics*, 31(2), 209–248. <https://doi.org/10.1017/S0022112068000133>
- Britter, R. E., & Linden, P. F. (1980). The motion of the front of a gravity current travelling down an incline. *Journal of Fluid Mechanics*, 99(3), 531–543. <https://doi.org/10.1017/S0022112080000754>
- Brothers, S., Kazanjian, G., Köhler, J., Scharfenberger, U., & Hilt, S. (2017). Convective mixing and high littoral production established systematic errors in the diel oxygen curves of a shallow, eutrophic lake. *Limnology and Oceanography: Methods*, 15(5), 429–435. <https://doi.org/10.1002/lom3.10169>
- Bühler, J., Wright, S. J., & Kim, Y. (1991). Gravity currents advancing into a coflowing fluid. *Journal of Hydraulic Research*, 29(2), 343–357. <https://doi.org/10.1080/00221689109499007>
- Cenedese, C., & Adduce, C. (2010). A new parameterization for entrainment in overflows. *Journal of Physical Oceanography*, 40(8), 1835–1850. <https://doi.org/10.1175/2010JPO4374.1>
- Chen, C. (1995). Numerical simulations of gravity currents in uniform shear flows. *Monthly Weather Review*, 123(11), 3240–3253. [https://doi.org/10.1175/1520-0493\(1995\)123<3240:NSOGCI>2.0.CO;2](https://doi.org/10.1175/1520-0493(1995)123<3240:NSOGCI>2.0.CO;2)
- Chen, C.-T. A., & Millero, F. J. (1986). Precise thermodynamic properties for natural waters covering only the limnological range. *Limnology & Oceanography*, 31(3), 657–662. <https://doi.org/10.4319/lo.1986.31.3.0657>
- Ching, C., Fernando, H., & Noh, Y. (1993). Interaction of a negatively buoyant line plume with a density interface. *Dynamics of Atmospheres and Oceans*, 19(1–4), 367–388. [https://doi.org/10.1016/0377-0265\(93\)90042-6](https://doi.org/10.1016/0377-0265(93)90042-6)
- Christodoulou, G. C. (1986). Interfacial mixing in stratified flows. *Journal of Hydraulic Research*, 24(2), 77–92. <https://doi.org/10.1080/00221688609499323>
- Chubarenko, I. P., Esiukova, E., Stepanova, N., Chubarenko, B., & Baudler, H. (2013). Down-slope cascading modulated by day/night variations of solar heating. *Journal of Limnology*, 72(2), e19. <https://doi.org/10.4081/jlimnol.2013.e19>
- Cotel, A. J., & Kudo, Y. (2008). Impingement of buoyancy-driven flows at a stratified interface. *Experiments in Fluids*, 45(1), 131–139. <https://doi.org/10.1007/s00348-008-0469-5>
- Cushman-Roisin, B. (1982). Penetrative convection in the upper ocean due to surface cooling. *Geophysical & Astrophysical Fluid Dynamics*, 19(1–2), 61–91. <https://doi.org/10.1080/03091928208208947>
- Dailey, P. S., & Fovell, R. G. (1999). Numerical simulation of the interaction between the sea-breeze front and horizontal convective rolls. Part I: Offshore ambient flow. *Monthly Weather Review*, 127(5), 858–878. [https://doi.org/10.1175/1520-0493\(1999\)127<0858:NSOTIB>2.0.CO;2](https://doi.org/10.1175/1520-0493(1999)127<0858:NSOTIB>2.0.CO;2)
- Deardorff, J. W., Willis, G. E., & Lilly, D. K. (1969). Laboratory investigation of non-steady penetrative convection. *Journal of Fluid Mechanics*, 35(1), 7–31. <https://doi.org/10.1017/S0022112069000942>
- Deardorff, J. W., Willis, G. E., & Stockton, B. H. (1980). Laboratory studies of the entrainment zone of a convectively mixed layer. *Journal of Fluid Mechanics*, 100(1), 41–64. <https://doi.org/10.1017/S0022112080001000>
- Doda, T., Ramón, C. L., Ulloa, H. N., Wüest, A., & Bouffard, D. (2022). Seasonality of density currents induced by differential cooling. *Hydrology and Earth System Sciences*, 26(2), 331–353. <https://doi.org/10.5194/hess-26-331-2022>
- Dressler, R. F. (1949). Mathematical solution of the problem of roll-waves in inclined open channels. *Communications on Pure and Applied Mathematics*, 2(2–3), 149–194. <https://doi.org/10.1002/cpa.3160020203>
- Ellison, T. H., & Turner, J. S. (1959). Turbulent entrainment in stratified flows. *Journal of Fluid Mechanics*, 6(3), 423–448. <https://doi.org/10.1017/S0022112059000738>
- Fer, I., Lemmin, U., & Thorpe, S. A. (2001). Cascading of water down the sloping sides of a deep lake in winter. *Geophysical Research Letters*, 28(10), 2093–2096. <https://doi.org/10.1029/2000GL012599>
- Fer, I., Lemmin, U., & Thorpe, S. A. (2002). Contribution of entrainment and vertical plumes to the winter cascading of cold shelf waters in a deep lake. *Limnology & Oceanography*, 47(2), 576–580. <https://doi.org/10.4319/lo.2002.47.2.0576>
- Folkard, A. M. (2000). Laboratory observations of interactions of forced plumes with stratified shear layers. *Fluid Dynamics Research*, 26(6), 355–375. [https://doi.org/10.1016/S0169-5983\(99\)00038-6](https://doi.org/10.1016/S0169-5983(99)00038-6)
- Fritts, D. C., & Alexander, M. J. (2003). Gravity wave dynamics and effects in the middle atmosphere. *Reviews of Geophysics*, 41(1), 1003. <https://doi.org/10.1029/2001RG000106>
- Hall, F. F., Edinger, J. G., & Neff, W. D. (1975). Convective plumes in the planetary boundary layer, investigated with an acoustic echo sounder. *Journal of Applied Meteorology*, 14(4), 513–523. [https://doi.org/10.1175/1520-0450\(1975\)014<0513:CPITPB>2.0.CO;2](https://doi.org/10.1175/1520-0450(1975)014<0513:CPITPB>2.0.CO;2)
- Harleman, D. R. F., & Ippen, A. T. (1960). The turbulent diffusion and convection of saline water in an idealised estuary. In International Association for Science of Hydrology, Commission of Surface Waters (Ed.), *Publ. No. 51* (pp. 362–378).
- Helfrich, K. R. (1995). Time-dependent two-layer hydraulic exchange flows. *Journal of Physical Oceanography*, 25(3), 359–373. [https://doi.org/10.1175/1520-0485\(1995\)025<0359:TDTLHE>2.0.CO;2](https://doi.org/10.1175/1520-0485(1995)025<0359:TDTLHE>2.0.CO;2)
- Hetzl, Y., Pattiaratchi, C., Lowe, R., & Hofmeister, R. (2015). Wind and tidal mixing controls on stratification and dense water outflows in a large hypersaline bay. *Journal of Geophysical Research: Oceans*, 120(9), 6034–6056. <https://doi.org/10.1002/2015JC010733>
- Hogg, A. J., Hallworth, M. A., & Huppert, H. E. (2005). On gravity currents driven by constant fluxes of saline and particle-laden fluid in the presence of a uniform flow. *Journal of Fluid Mechanics*, 539, 349–385. <https://doi.org/10.1017/S002211200500546X>
- Hogg, A. M., Ivey, G. N., & Winters, K. B. (2001). Hydraulics and mixing in controlled exchange flows. *Journal of Geophysical Research*, 106(C1), 959–972. <https://doi.org/10.1029/2000JC000266>
- Horsch, G. M., & Stefan, H. G. (1988). Convective circulation in littoral water due to surface cooling. *Limnology & Oceanography*, 33(5), 1068–1083. <https://doi.org/10.4319/lo.1988.33.5.1068>

- Huang, H., Imran, J., Pirmez, C., Zhang, Q., & Chen, G. (2009). The critical densimetric Froude number of subaqueous gravity currents can be non-unity or non-existent. *Journal of Sedimentary Research*, 79(7), 479–485. <https://doi.org/10.2110/jsr.2009.048>
- Huppert, H. E. (2006). Gravity currents: A personal perspective. *Journal of Fluid Mechanics*, 554, 299–322. <https://doi.org/10.1017/S002211200600930X>
- Huppert, H. E., Turner, J., Carey, S. N., Stephen, R., Sparks, J., & Hallworth, M. A. (1986). A laboratory simulation of pyroclastic flows down slopes. *Journal of Volcanology and Geothermal Research*, 30(3–4), 179–199. [https://doi.org/10.1016/0377-0273\(86\)90054-5](https://doi.org/10.1016/0377-0273(86)90054-5)
- Imberger, J. (1985). The diurnal mixed layer. *Limnology & Oceanography*, 30(4), 737–770. <https://doi.org/10.4319/lo.1985.30.4.0737>
- Linden, P. F., & Simpson, J. E. (1986). Gravity-driven flows in a turbulent fluid. *Journal of Fluid Mechanics*, 172, 481–497. <https://doi.org/10.1017/S0022112086001829>
- Lofquist, K. (1960). Flow and stress near an interface between stratified liquids. *Physics of Fluids*, 3(2), 158–175. <https://doi.org/10.1063/1.1706013>
- Mahjabin, T., Pattiaratchi, C., & Hetzel, Y. (2019). Wind effects on dense shelf water cascades in south-west Australia. *Continental Shelf Research*, 189, 103975. <https://doi.org/10.1016/j.csr.2019.103975>
- Maxworthy, T. (1983). The dynamics of double-diffusive gravity currents. *Journal of Fluid Mechanics*, 128, 259–282. <https://doi.org/10.1017/S0022112083000488>
- Middleton, G. V. (1966). Experiments on density and turbidity currents. II. Uniform flow of density currents. *Canadian Journal of Earth Sciences*, 3(5), 627–637. <https://doi.org/10.1139/e66-044>
- Miles, J. W. (1961). On the stability of heterogeneous shear flows. *Journal of Fluid Mechanics*, 10(4), 496–508. <https://doi.org/10.1017/S0022112061000305>
- Monismith, S. G., Imberger, J., & Morison, M. L. (1990). Convective motions in the sidearm of a small reservoir. *Limnology & Oceanography*, 35(8), 1676–1702. <https://doi.org/10.4319/lo.1990.35.8.1676>
- Moore, M. J., & Long, R. R. (1971). An experimental investigation of turbulent stratified shearing flow. *Journal of Fluid Mechanics*, 49(4), 635–655. <https://doi.org/10.1017/S0022112071002301>
- Needham, D. J., & Merkin, J. H. (1984). On roll waves down an open inclined channel. *Proceedings of the Royal Society of London A*, 394, 259–278. <https://doi.org/10.1098/rspa.1984.0079>
- Noh, Y., Fernando, H. J. S., & Ching, C. Y. (1992). Flows induced by the impingement of a two-dimensional thermal on a density interface. *Journal of Physical Oceanography*, 22(10), 1207–1220. [https://doi.org/10.1175/1520-0485\(1992\)022<1207:FIBTIO>2.0.CO;2](https://doi.org/10.1175/1520-0485(1992)022<1207:FIBTIO>2.0.CO;2)
- Ogawa, S., Sha, W., Iwasaki, T., & Wang, Z. (2003). A numerical study on the interaction of a sea-breeze front with convective cells in the daytime boundary layer. *Journal of the Meteorological Society of Japan. Ser. II*, 81(4), 635–651. <https://doi.org/10.2151/jmsj.81.635>
- Parker, D. J., Burton, R. R., Diongue-Niang, A., Ellis, R. J., Felton, M., Taylor, C. M., et al. (2005). The diurnal cycle of the West African monsoon circulation. *Quarterly Journal of the Royal Meteorological Society*, 131(611), 2839–2860. <https://doi.org/10.1256/qj.04.52>
- Pawlak, G., & Armi, L. (2000). Mixing and entrainment in developing stratified currents. *Journal of Fluid Mechanics*, 424, 45–73. <https://doi.org/10.1017/S0022112000001877>
- Ramón, C. L., Ulloa, H. N., Doda, T., & Bouffard, D. (2022). Flushing the lake littoral region: The interaction of differential cooling and mild winds. *Water Resources Research*, 58(3), e2021WR030943. <https://doi.org/10.1029/2021WR030943>
- Safaie, A., Pawlak, G., & Davis, K. A. (2022). Diurnal thermally driven cross-shore exchange in steady alongshore currents. *Journal of Geophysical Research: Oceans*, 127(4), e2021JC017912. <https://doi.org/10.1029/2021JC017912>
- Salinas, J., Balachandrar, S., Shringarpure, M., Fedele, J., Hoyal, D., & Cantero, M. (2020). Soft transition between subcritical and supercritical currents through intermittent cascading interfacial instabilities. *Proceedings of the National Academy of Sciences*, 117(31), 18278–18284. <https://doi.org/10.1073/pnas.2008959117>
- Serafin, S., & Zardi, D. (2010). Daytime heat transfer processes related to slope flows and turbulent convection in an idealized mountain valley. *Journal of the Atmospheric Sciences*, 67(11), 3739–3756. <https://doi.org/10.1175/2010JAS3428.1>
- Sha, W., Kawamura, T., & Ueda, H. (1991). A numerical study on sea/land breezes as a gravity current: Kelvin–Helmholtz billows and inland penetration of the sea-breeze front. *Journal of the Atmospheric Sciences*, 48(14), 1649–1665. [https://doi.org/10.1175/1520-0469\(1991\)048<1649:ANSOSB>2.0.CO;2](https://doi.org/10.1175/1520-0469(1991)048<1649:ANSOSB>2.0.CO;2)
- Simpson, J. E. (1982). Gravity currents in the laboratory, atmosphere, and ocean. *Annual Review of Fluid Mechanics*, 14(1), 213–234. <https://doi.org/10.1146/annurev.fl.14.010182.001241>
- Simpson, J. E. (1986). Mixing at the front of a gravity current. *Acta Mechanica*, 63(1–4), 245–253. <https://doi.org/10.1007/BF01182551>
- Simpson, J. E., & Britter, R. E. (1980). A laboratory model of an atmospheric mesofront. *Quarterly Journal of the Royal Meteorological Society*, 106(449), 485–500. <https://doi.org/10.1002/qj.49710644907>
- Simpson, J. E., Mansfield, D. A., & Milford, J. R. (1977). Inland penetration of sea-breeze fronts. *Quarterly Journal of the Royal Meteorological Society*, 103(435), 47–76. <https://doi.org/10.1002/qj.49710343504>
- Stull, R. B. (1976). Internal gravity waves generated by penetrative convection. *Journal of the Atmospheric Sciences*, 33(7), 1279–1286. [https://doi.org/10.1175/1520-0469\(1976\)033<1279:IGWGBP>2.0.CO;2](https://doi.org/10.1175/1520-0469(1976)033<1279:IGWGBP>2.0.CO;2)
- Sullivan, P. P., Moeng, C.-H., Stevens, B., Lenschow, D. H., & Mayor, S. D. (1998). Structure of the entrainment zone capping the convective atmospheric boundary layer. *Journal of the Atmospheric Sciences*, 55(19), 3042–3064. [https://doi.org/10.1175/1520-0469\(1998\)055<3042:SOTEZC>2.0.CO;2](https://doi.org/10.1175/1520-0469(1998)055<3042:SOTEZC>2.0.CO;2)
- Thorpe, S. A., & Ozen, B. (2007). Are cascading flows stable? *Journal of Fluid Mechanics*, 589, 411–432. <https://doi.org/10.1017/S0022112007007902>
- Ulloa, H. N., Ramón, C. L., Doda, T., Wüest, A., & Bouffard, D. (2022). Development of overturning circulation in sloping waterbodies due to surface cooling. *Journal of Fluid Mechanics*, 930, A18. <https://doi.org/10.1017/jfm.2021.883>
- Veronis, G. (1963). Penetrative convection. *The Astrophysical Journal*, 137, 641–663. <https://doi.org/10.1086/147538>
- Waltham, D. (2004). Flow transformations in particulate gravity currents. *Journal of Sedimentary Research*, 74(1), 129–134. <https://doi.org/10.1306/062303740129>
- Wells, M. G., & Dorrell, R. M. (2021). Turbulence processes within turbidity currents. *Annual Review of Fluid Mechanics*, 53(1), 59–83. <https://doi.org/10.1146/annurev-fluid-010719-060309>
- Winters, K. B., & Seim, H. E. (2000). The role of dissipation and mixing in exchange flow through a contracting channel. *Journal of Fluid Mechanics*, 407, 265–290. <https://doi.org/10.1017/S0022112099007727>
- Wright, L. D., Friedrichs, C. T., Kim, S. C., & Scully, M. E. (2001). Effects of ambient currents and waves on gravity-driven sediment transport on continental shelves. *Marine Geology*, 175(1–4), 25–45. [https://doi.org/10.1016/S0025-3227\(01\)00140-2](https://doi.org/10.1016/S0025-3227(01)00140-2)
- Zhu, D. Z., & Lawrence, G. A. (2001). Holmboe's instability in exchange flows. *Journal of Fluid Mechanics*, 429, 391–409. <https://doi.org/10.1017/S002211200000286X>